MTLA 27 (2023) 101675

Contents lists available at ScienceDirect

Materialia

journal homepage: www.elsevier.com/locate/mtla

Full Length Article

In-situ, real-time investigation of the formation of oxygen-containing rare-earth hydrides by combining a quartz crystal microbalance and ion beam analysis

E. Pitthan [a,*], C. Cupak [b], M. Fellinger [b], M.V. Moro [a], S. Kioumourtzoglou [a], D. Moldarev [a], M. Wolff [a], F. Aumayr [b], D. Primetzhofer [a]

[a] Department of Physics and Astronomy, Ångström Laboratory, Uppsala University, Box 516, SE-751 20 Uppsala, Sweden
[b] TU Wien, Institute of Applied Physics, Fusion@ÖAW, 1040 Vienna, Austria

ARTICLE INFO

Keywords:
Photochromic films
Oxygen-containing yttrium-hydride
Oxygen-containing gadolinium-hydride
Quartz crystal microbalance
Ion beam analysis

ABSTRACT

We present an in-situ and real-time investigation of the formation of YHO and GdHO thin films grown by reactive e^--beam evaporation. Mass changes were continuously monitored during deposition, oxidation, and illumination using a highly sensitive quartz crystal microbalance, while changes in chemical composition and depth profiles were investigated simultaneously by ion beam analysis. Results highlight the strong reactivity of freshly deposited YH_x and GdH_x films, even under ultra-high vacuum conditions. Oxidation starts at the surfaces of the films and the oxidation rate is strongly dependent on the O_2 pressure. The response of the system under ion beam irradiation and in-situ illumination is also presented and discussed. For the measured mass changes, a quantitative agreement better than 2% was observed between both techniques and demonstrates the consistency and sensitivity of this approach.

1. Introduction

Oxygen-containing rare-earth metal-hydride (REMHO) thin films such as YHO, GdHO, DyHO, and NdHO can present reversible modification of their optical transmittance under illumination, referred to as photochromism [1–3]. The effect is observed at room temperatures and ambient conditions [1,4], making the materials outstanding candidates for passive smart window applications and optoelectronic devices as gas sensors. Typically, REMHO films are synthesized in a two-step process: i) First, an opaque thin film of a rare earth metal (REM) dihydride (such as YH_2) is formed on a substrate by either reactive magnetron sputtering [5,6] or e^--beam evaporation [7]. ii) Second, the film is oxidized, by either venting the vacuum chamber or in a controlled oxygen atmosphere. The resulting REMHO films are transparent and photochromic [3,8,9]. The ratio between oxygen and REM has been shown to play a major role for the photochromic contrast: the oxygen incorporation results in hydrogen loss [7,9] and photochromism is observed for atomic ratios O/REM in the range of 0.45 to 1.5 [3,10,11].

Despite the high potential for technological application, the exact synthesis pathways of REMHO and their effects on the photochromic response are not sufficiently understood. Recently, the synthesis of YHO films grown by e^--beam evaporation was investigated in-situ by ion beam analysis (IBA), allowing to obtain the film composition and elemental depth profile before and after oxidation [7]. It was shown that initially, indeed YH_2 is formed, which is subsequently oxidized. Studies with $^{16}O/^{18}O$ labeling show no significant mobility of oxygen within the film after oxidation [12]. Our studies which used different deposition techniques also indicate a dependence on the resulting microstructure of the film [7,10]. These preliminary results suggest that specific details of the formation of REMHO thin films and the evolution of their composition under controlled conditions, such as deposition rate and oxygen exposure will provide further insight into the photochromic mechanism and on how to control the optical properties of the system. Although IBA allows to evaluate the film composition in-situ at specific synthesis steps (*i.e.* before and after oxidation), real-time monitoring of mass modification is not possible but highly desirable to understand the film growth, oxidation and hydrogen release processes. Material modification from ion irradiation might also to a certain extend affect the characterization of these films as previous studies indicate that the films can be subject to hydrogen loss during IBA [9]. Monitoring the mass change of the

* Corresponding author.
E-mail address: eduardo.pitthan@physics.uu.se (E. Pitthan).

https://doi.org/10.1016/j.mtla.2023.101675
Received 12 October 2022; Received in revised form 10 December 2022; Accepted 3 January 2023
Available online 4 January 2023

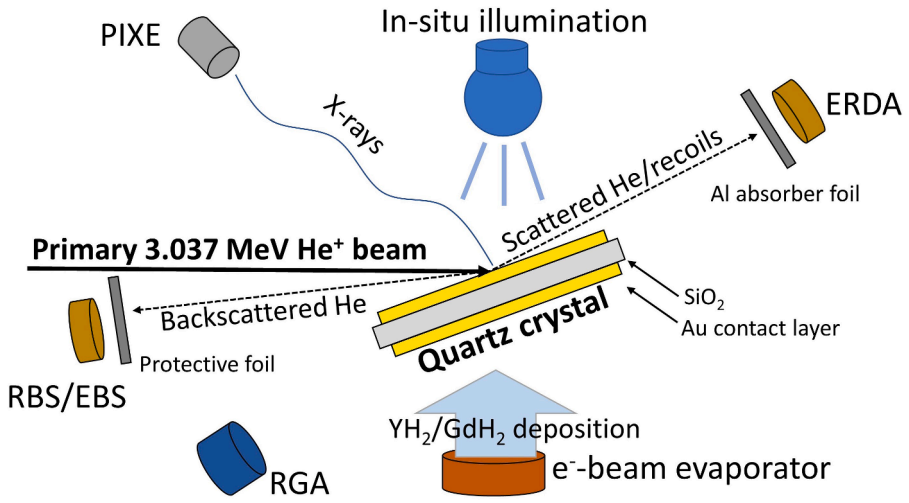

Fig. 1. Sketch of the experimental set-up used for YH_2/GdH_2 film deposition on a QC in combination with in-situ oxidation and characterization with QCM, RGA, and IBA. The QC can be rotated to meet the geometrical configurations as necessary for the individual experimental techniques.

samples of interest allows to track such potential effects induced by ion irradiation and during the illumination with light (photochromic response) [9,13].

In this work, YH_x and GdH_x films were grown by e^--beam evaporation using quartz crystals (QC) as substrate. This approach allows the use of a highly sensitive quartz crystal microbalance (QCM) to monitor the mass modification during the entire synthesis process, *i.e.*, film deposition and controlled oxidation under different conditions in real-time. In parallel, in-situ film characterization by IBA was performed to correlate the mass modifications observed by the QCM with the composition of the films. A quantitative comparison between QCM and IBA is performed, resulting in an agreement for the mass changes better than 2%. The behavior of the QCM signal during IBA and in-situ illumination is also investigated and discussed.

2. Instrument and system configuration

The in-situ investigations were performed in SIGMA (Set-up for In-situ Growth, Material modification and Analysis) [14], located at the 5 MV Tandem accelerator at Uppsala University [15]. The set-up allows the deposition of a wide range of materials by inert and reactive thin film growth using e^--beam evaporation, besides thermal treatment and ion implantation. The growth process can be verified by in-situ IBA characterization without breaking the vacuum. Films were synthesized in ultra-high vacuum, while in-situ IBA characterization was performed by Elastic Backscattering Spectrometry (EBS) and Elastic Recoil Detection Analysis (ERDA) after each synthesis step. Additionally, Particle-Induced X-Ray Emission (PIXE) was also performed using the same beam to identify heavier constituents. The sample holder was rotated to a specific geometry for each synthesis and analysis step (more details on the system in [14]). Recently, a highly sensitive QCM that allows detection of net mass changes by a quartz resonator was installed, allowing real time and in-situ investigation of film deposition and modification. The system was developed at TU Wien, based on the design from G. Hayderer et al. [16]. Relative changes in the mass $\Delta m/m$ are calculated by the relative change in the resonance frequency $\Delta f/f$ as described by the Sauerbrey equation [17],

$$-\frac{\Delta f}{f} = \frac{\Delta m}{m}. \quad (1)$$

Eq. (1) combines mass changes and eigenfrequency changes of a given quartz crystal and holds true for film thicknesses sufficiently thinner than the thickness of the quartz crystal. Dedicated electronics were designed to enable real-time calculations of mass changes by recording the Quartz Crystal's eigenfrequency throughout the experiment. A mass change in the order of 10 pg cm^{-2} s^{-1} [16,18,19] can be traced. Commercial QC's (SC-cut) with 14 mm diameter and 0.3 mm thickness were used as substrates, acquired from the company KVG Quartz Crystal Technology GmbH, Germany. Gold electrodes with 140 nm thickness on each side are applied as electrical contact with a Cr buffer layer used between Au and QC. To avoid an overlapping of the Gd and Au signal in the EBS spectra, Al films of 365 nm thickness and 8.55 mm diameter in the center of the crystal were grown by magnetron sputtering (MED 010, Balzers Union) on the QC before loading them into the SIGMA chamber. The argon pressure during Al film deposition was 1×10^{-2} mbar and the current was 50 mA, resulting in a growth rate of 2 Å/s. Yttrium hydride (YH_x) and gadolinium hydride (GdH_x) films were grown by reactive e^--beam evaporation using a commercial metallic yttrium target (99% nominal purity) from a tungsten crucible and a gadolinium target (elemental analysis from x-ray fluorescence measurements indicate mainly Gd with small traces of Fe) from a tantalum crucible, respectively, in a reactive hydrogen atmosphere (kept constant at 1×10^{-6} and 3×10^{-6} mbar for YH_x and GdH_x, respectively) using a triple source e^--beam evaporator (FOCUS EFM 3T) with a distance of around 100 mm between sample and evaporator. The targets were degassed prior to evaporation and the base pressure in the chamber before growth was lower than 5×10^{-8} mbar. Subsequently, oxygen was introduced in the chamber by a controlled flux via a leak valve, up to the desired pressure to oxidize the films. The gas composition was monitored by a Pfeiffer QMG 250 F1 PrismaPro residual gas analyzer (RGA) for pressures below 1×10^{-4} mbar. All experiments were performed at room temperature. The experimental set-up at SIGMA used in this work is schematically represented in Fig. 1.

IBA was performed using a He^+ beam at 3.037 MeV. For oxygen detection, EBS was performed with normal incidence to the sample surface (0° incident angle) with the detector placed at a scattering angle of 170° (solid angle of 2.08×10^{-3} sr, covered with a foil of ~139 nm Au and 44 nm C) and using the narrow (≈10 keV) elastic resonance of $^{16}O(\alpha,\alpha_0)^{16}O$ at 3.037 MeV [20]. The amounts of Y, Gd, Al, and Au were quantified from these measurements as well. For hydrogen quantification, ERDA was performed at 70° incident angle to the sample surface and a scattering angle of 30° (solid angle of 3.46×10^{-3} sr) with respect to the beam direction. Hydrogen recoils from the sample were detected, while scattered primary ions as well as other recoiling species were stopped by an Al absorber foil with a thickness of 10.3 μm placed in front of the detector. ERDA spectra were normalized by the charge-solid angle product using the substrate signal from the RBS spectra. The RBS/EBS and ERDA fits were performed using SIMNRA [21] with $^{16}O(\alpha,\alpha_0)^{16}O$

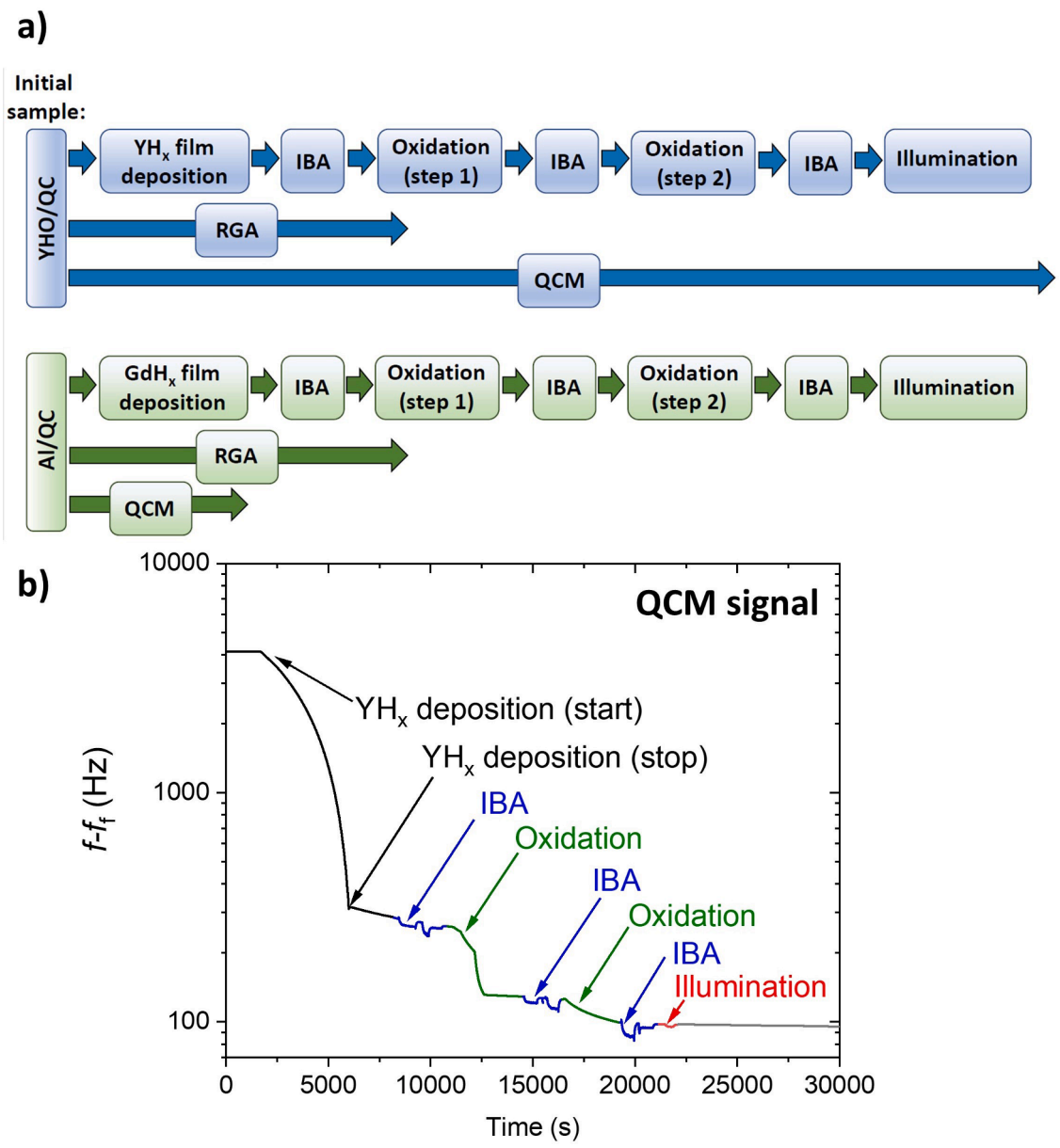

Fig. 2. **a)** Flowchart illustrating the sequence of sample preparation and analysis in this work. **b)** QCM signal obtained during YH_x deposition on an initial template sample of YHO/QC followed by different steps as described in the flowchart (f_f is the final frequency of the experiment).

and $^1H(\alpha,p)^4He$ elastic scattering and recoil cross sections from SigmaCalc [22]. For in-situ illumination of the films a LED-cluster ($\lambda = 455$ nm and power = 4.865 W), positioned outside the chamber, was facing the sample through a window. Ex-situ IBA characterization was also performed by Time-of-Flight ERDA (ToF-ERDA) using two carbon foils for the time-of-flight measurement and a gas ionization chamber for the energy signal placed at 45° with respect to the beam direction [15]. 36 MeV I^{8+} served as probing species and depth profiles were obtained from the recoil spectra using the CONTES code [23].

Fig. 2a presents a flowchart of the experiments. Growth of YH_x was performed on a thin YHO film pre-deposited on a QC, initially used to optimize evaporation and QCM parameters. The film growth was followed by two oxidation steps under different oxygen pressures. After YH_x growth and after each oxidation step the composition of the film was extracted from EBS and ERDA. The mass of the films was monitored by QCM during the entire experiment. The resulting QCM signal for the experiment, including film deposition, different IBA and oxidation steps and illumination, is presented in Fig. 2b. GdH_x was grown on Al/QC structures to ensure signal separation in EBS between Gd and the Au film used as electrical contact. QCM monitoring was interrupted after growth of the GdH_x film due to interference in the signal. The growth of the GdH_x film was followed by two oxidation steps, and composition modification was studied by IBA.

A typical QCM signal during IBA and illumination is presented in Fig. 3. A spike to higher frequencies is observed at the moment the MeV beam hits the center of the crystal, followed by a continuous decrease in frequency. An inverse behavior is observed at the moment the MeV beam is turned off, with a spike to lower frequencies followed by an increase in frequency that, after a few minutes, reaches similar frequency values as before the beam was switched on. While the frequency spikes observed in association with switching the beam on and off are attributed to the change in momentum transfer from the energetic ions, the slow decrease in frequency during IBA is attributed to a temperature increase. During illumination, a decrease in frequency is observed, attributed to a heating of the system from the light source, similar to the energy deposition by the ion beam. After the illumination is stopped, the

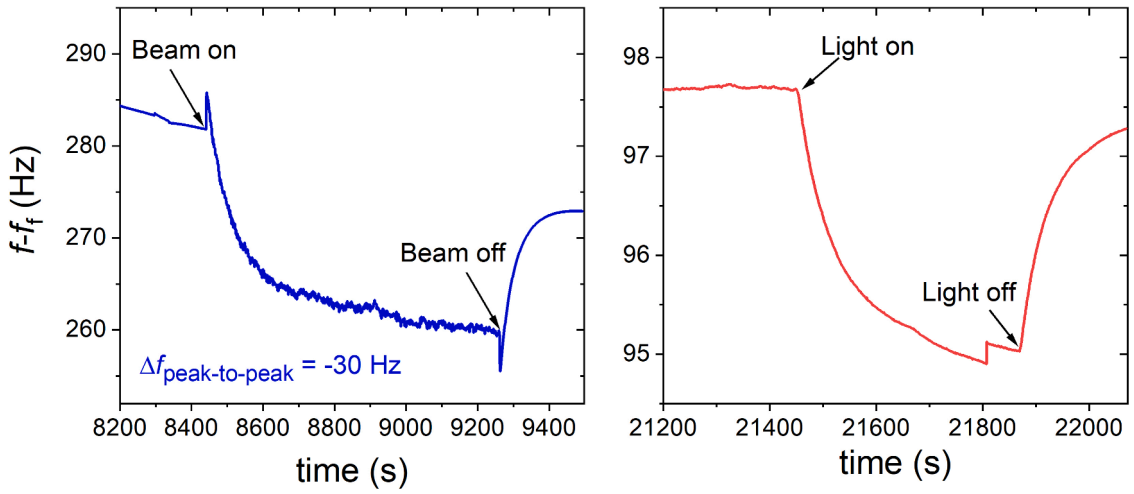

Fig. 3. (left) Typical QCM signal obtained during IBA using a He^+ 3.037 MeV primary beam in normal incidence and a current in the range of a few nA. (right) QCM signal for YHO/QC during an in-situ illumination using a 455 nm wavelength light source.

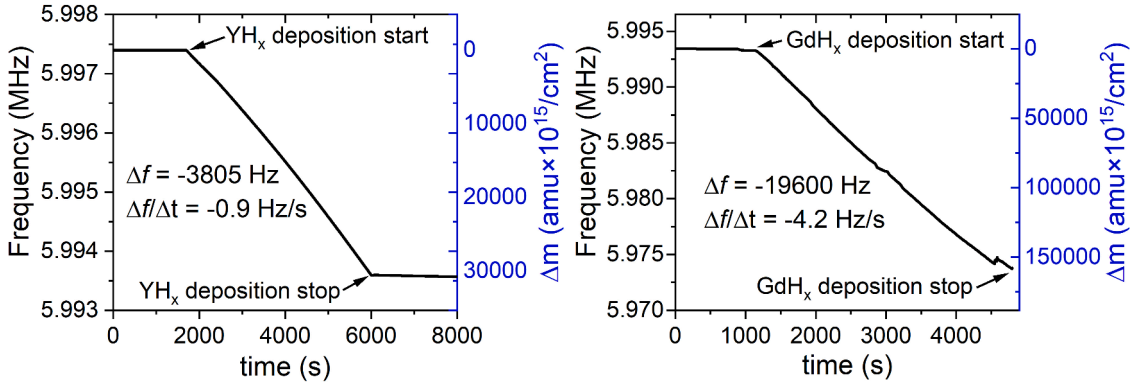

Fig. 4. QCM signal before, during and after the deposition of (left) YH_x and (right) GdH_x.

signal converges back to similar frequency values from before illumination. Since the frequency changes reverse towards the initial trends both after the exposure to the MeV beam and the light source, no strong effects from these techniques on the total mass and therefore stoichiometry of the sample were expected to be relevant in our study. Release of loosely bound hydrogen was, however, previously observed from REMHO films during the first darkening/bleaching cycle [13]. Such mass loss would result in an increase in frequency after illumination, which was not observed in our case mainly due to the slow but continuous oxidation process taking place even in vacuum conditions, as discussed below.

3. Results and discussion

3.1. Film deposition

Using the QCM system, real-time frequency and mass change monitoring was performed during YH_x and GdH_x film deposition as presented in Fig. 4. This allows to verify the deposition rates as well as to estimate final film thicknesses. A mass gain per unit area ($\Delta m/A$) of $30{,}554\times10^{15}$ and $157{,}388\times10^{15}$ amu/cm^2 for YH_x and GdH_x, respectively, is obtained by using Eq. (1). These values correspond to an YH_2 areal density of 336.1×10^{15} atoms/cm^2 (approximately 40 nm, considering mass density from density functional theory calculations [24]) and a GdH_2 areal density of 988.3×10^{15} atoms/cm^2 (approximately 110 nm, considering Gd mass density). Considering also the previously deposited YHO and Al films on top of the initial crystal substrates, maximum thicknesses did not exceed 500 nm, being orders of magnitude thinner than the quartz thickness itself and, therefore, holding valid mass and frequency relations from Eq. (1). A detailed comparison between areal densities obtained by QCM and IBA considering film lateral homogeneity is presented later in this work.

3.2. Controlled oxidation

An EBS spectrum recorded after YH_x deposition is presented in Fig. 5a. The O/Y ratio of 0.41 for the as-deposited layer already indicates a significant presence of oxygen. Besides possible oxidation during deposition, the strong oxidation tendency of the thin film even in ultra-high vacuum conditions (pressure of around 5×10^{-8} mbar and partial pressure of water vapor and O_2 of 11×10^{-9} and 0.7×10^{-9} mbar, respectively) is evidenced by the QCM immediately after the deposition is interrupted, as presented in Fig. 5b. Initially, an excursion in frequency is observed, attributed to a temperature variation from the film deposition interruption, that resulted in a decrease in $\Delta m/A$ observed in Fig. 5b from the direct conversion of frequency to mass changes. This is followed by a roughly constant mass increase with a $\frac{\Delta m}{A*t}$ rate of 0.126×10^{15} amu/cm^2/s due to the film oxidation. Once O_2 is introduced in the chamber, this rate increases significantly and is dependent on the O_2 pressure, as seen clearly in Fig. 5c. After each increase of O_2 pressure, an exponentially decaying trend in mass increase can be seen. Oxidation step 1 resulted in a total O_2 exposure dose of 4.10×10^4 Langmuir (L), while oxidation step 2 resulted in an exposure of 29.3×10^4 L. EBS data presented in Fig. 5a evidenced the O/Y atomic ratio increase from 0.41

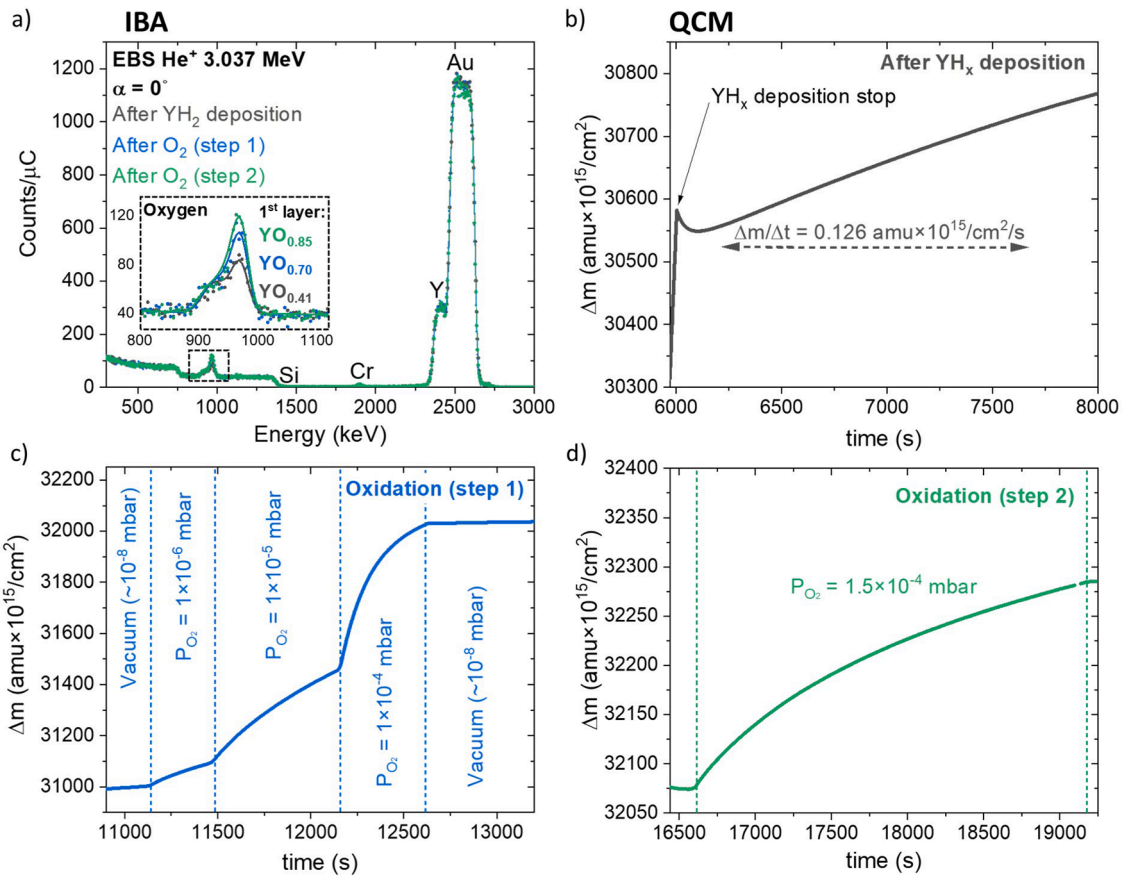

Fig. 5. a) EBS spectra for the YHO/QC structure after the YH_x deposition and different oxidation steps. b) QCM signal immediately after YH_x deposition and (c) during 1st and (d) 2nd oxidation step.

Table 1
Oxygen pressure, oxygen dose in Langmuir, mass per area increase, and initial and final sticking coefficient for different steps extracted from Fig 5b and 5c.

P_{O2} (mbar)	L ($\times 10^4$)	$\Delta m/A$ (amu$\times 10^{15}$/cm^2)	S_i	S_f
1.2×10^{-8}*	0.00036	450	0.54	0.55
1.0×10^{-6}	0.025	91	0.041	0.024
1.0×10^{-5}	0.51	362	0.0092	0.0041
1.0×10^{-4}	3.6	568	0.0031	0.00040

* Considering partial pressure from oxygen and water vapor from RGA signal.

to 0.70 after oxidation step 1. The oxidation rate is significantly decreased during oxidation step 2 (Fig. 5d), even after exposure to higher O_2 doses, resulting in a final O/Y ratio of 0.85. Such results evidenced that the initially observed oxidation tendency is significantly reduced as the O/Y ratios get closer to unity, suggesting an exponentially decaying saturation process. Oxygen incorporation in the thin films can also be described in terms of a sticking coefficient (S). Table 1 shows the $\Delta m/A$ and S calculated from the QCM signal for the different oxygen pressures and doses during oxidation step 1, as presented in Fig. 5c. S is calculated from the ratio of the number of incorporated oxygen atoms (based on mass gain calculated from the QCM signal) per time to the number of atoms that impinges the surface per time (approximated from [25] for a temperature of 22°C). A strong mass gain at vacuum conditions is evidenced right after the deposition of the film (450 amu$\times 10^{15}$/cm^2 for a dose of 36 L). The stable S value of 0.55 during this stage is a result of an approximately constant oxygen incorporation rate taking place mainly at the surface region of the film. The increase of oxygen pressure results in an increase of mass gain rate (Fig. 5c) which is, however, accompanied with a significant reduction of S as oxidation advances (Table 1). This reduction in S, at increased oxygen exposure and thus higher impinging rate of oxygen on the surface, is consistent with diffusion-limited oxidation, taking place as O/Y ratios increases. Considering the oxidation process consisting of several steps, each with a characteristic rate, such as the oxygen influx, adsorption, dissociation, diffusion and reaction, different limiting factors are expected to be observed at different stages of the oxidation process. It was previously observed that this O/Y ratio can increase continuously over time for samples exposed to air, reaching O/Y ratios up to 2.1 after several months [9].

As a next step, the results on Gd deposition are shown. An EBS spectrum recorded for the QC (Au electrical contact/Cr buffer layer/SiO_2 crystal) used as substrate with the sputtered Al film on top is presented in Fig. 6, including the spectra after the deposition of the GdH_x film, as well as after two sequential oxidation steps (dose of 6.8×10^4 and 92.2×10^4 L for the first and second step, respectively). A SIMNRA simulation not considering the Al film is also presented to demonstrate the signal overlap between Gd and Au, which would have complicated the data analysis. The uniform plateau after film growth and a low oxygen content indicate a homogeneous oxygen-free film. The non-uniform plateau observed for the Gd signal after first oxidation evidences that the oxidation starts at the film surface, until the entire film is homogeneously oxidized, resulting in a Gd step signal as observed after the second oxidation step. As mentioned earlier, the detection of oxygen by EBS is very surface sensitive due to the resonant $^{16}O(\alpha,\alpha_0)^{16}O$ scattering cross section for the selected probing beam energy. This explains the similar oxygen spectra for both oxidation steps as seen in Fig. 6, further supporting the explanation that oxidation starts and rapidly saturates at the surface. Nevertheless, after the second oxidation step, an increase in oxygen signal is observed at lower energies (around 880 keV), confirming the oxidation into deeper regions of the film via

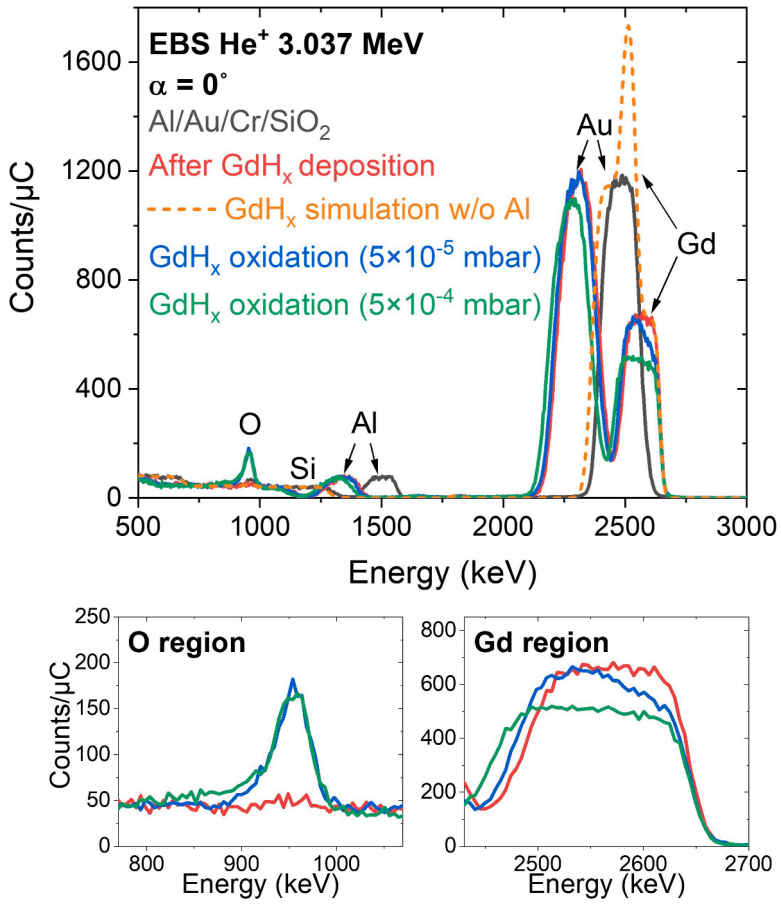

Fig. 6. EBS spectra for the GdH_x/Al/QC structure prior and after a series of oxidation steps (SIMNRA simulation of GdH_x/QC without Al film is presented for comparison).

diffusion.

3.3. Quantitative comparison of IBA and QCM

Film homogeneity must be considered when comparing quantitative results from IBA and QCM, accounting for potential inhomogeneity in thickness and composition. The radial sensitivity of a QCM can be described by a Gaussian profile with a FWHM of 1.6 mm in the center of the crystal, which effectively results in a sensitive area of about 4 mm diameter [26,27]. The IBA beam spots used show a diameter of approximately 1 mm, defined by a set of slits at the chamber entrance. To quantitatively compare the $\Delta m/A$ values obtained by QCM with areal densities obtained by IBA, a GdH_xO_y film was grown and characterized in-situ. IBA results show that a film with composition of $GdH_{1.84}O$ and areal density of 540×10^{15} atoms/cm^2, corresponding to $24{,}620\times10^{15}$ amu/cm^2, was deposited on top of the crystal. QCM resulted in a total $\Delta m/A$ of $24{,}280\times10^{15}$, with a relative difference of 1.38% in comparison to the IBA result, demonstrating the excellent agreement between the independent measurements.

To verify that the agreement of $\Delta m/A$ between both techniques is not affected by possible inhomogeneity from the deposited film, compositional and thickness homogeneity of the GdH_xO_y/Al/QC structure were evaluated ex-situ. Composition of the film after 53 days of air exposure was obtained by ToF-ERDA. Although changes in composition in the film are possible due to air exposure, no loss of Gd is expected, which is dominating the mass on the GdHO films. Five different sample positions (1 mm spacing between each position) were measured around the center of the crystal. The analysis resulted in very similar composition for all positions: Gd atomic content varied from 23.7 to 24.2%, H from 9.4 to 11.0%, and O from 64.7 to 66.5%, with a film average

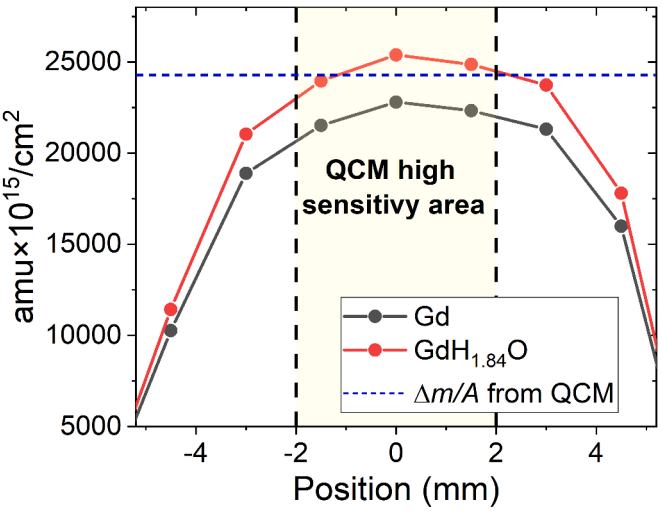

Fig. 7. Areal mass variation obtained by QCM after GdH_x deposition in comparison to ex-situ EBS measurement (He^+ at 3.037 MeV at $\alpha = 0$) on different positions around the center of the QC substrate (0 mm). The Gd mass, as well as the calculated mass considering the GdHO stoichiometry obtained by in-situ IBA measurements, are presented for comparison.

stoichiometry of $GdH_{0.42}O_{2.75}$. The O/H ratio was significantly higher in comparison to the composition obtained by in-situ analysis, as expected due to the continued oxidation/hydrogen loss in air. A higher (H+O)/Gd ratio than typically obtained for sputter-deposited films [3,10] is also

observed and is attributed to the low density of e^--beam deposited films resulting in increased adsorption of water molecules [7]. The homogeneity of the Gd areal density was furthermore evaluated using EBS at 0° of incident angle using the five-axis goniometer in the SIGMA set-up [14] to control the translation of the sample in relation to the beam. Au and Al areal densities were also evaluated to obtain the coordinates for the center of the crystal (named as 0 mm position). The value for $\Delta m/A$ of Gd along a linear profile across the center of the crystal is presented in Fig. 7 in comparison with $\Delta m/A$ obtained by the QCM. Gd corresponds to 90% of the mass from a GdHO film, and it results in a $\Delta m/A$ average within the QCM sensitivity area of 8.50% lower than the value obtained by the QCM. Supposing that the film composition obtained in-situ ($GdH_{1.84}O$) applies for the entire film area, the $\Delta m/A$ average within the QCM sensitivity area (Fig. 7) is only 1.89% higher than the value obtained by the QCM, confirming excellent agreement between both techniques.

4. Summary and conclusion

The formation of YHO and GdHO films was investigated in-situ and in real-time using a combination of a QCM system and IBA. The present approach allows to monitor mass modification during deposition, oxidation, and illumination, while correlating it to changes in the chemical composition of thin films. Highly reactive YH_x films were deposited and a strong dependence of the oxidation rate on the oxygen pressure was monitored. The oxidation slows down as the ratio of O/Y increases, reaching up to 0.85 after an oxygen dose of 33.4×10^4 L. IBA results indicate that oxidation starts at the film surface and progresses into the film until the whole layer is homogeneously oxidized. Our method allows in-situ monitoring of deposition and oxidation and by this it provides a pathway for tailored design of photochromic films with optimized performance. Quantitative analysis resulted in an agreement of better than 2% for the total mass change measured by QCM and IBA, demonstrating the potential of the present approach. The present study demonstrates the advantageous combination of the two methods yields additional quantitative information not directly available from the individual methods, which can be used for quantitative analysis of gas retention, oxidation or thin film decomposition processes under thermal load.

Declaration of Competing Interest

The authors declare that they have no known competing financial interests or personal relationships that could have appeared to influence the work reported in this paper.

Acknowledgements

This work has been carried out within the framework of the EUROfusion Consortium, funded by the European Union via the Euratom Research and Training Programme (Grant Agreement No 101052200 — EUROfusion). Views and opinions expressed are however those of the author(s) only and do not necessarily reflect those of the European Union or the European Commission. Neither the European Union nor the European Commission can be held responsible for them. Accelerator operation was supported by the Swedish Research Council VR-RFI, contracts #2019-00191 and #2017-00646_9, and the Swedish Foundation for Strategic Research (SSF) under contract RIF14-0053.

References

[1] T. Mongstad, C. Platzer-Bjorkman, J.P. Maehlen, L.P.A. Mooij, Y. Pivak, B. Dam, E. S. Marstein, B.C. Hauback, S.Zh. Karazhanov, A new thin film photochromic material: oxygen-containing yttrium hydride, Sol. Energy Mater. Sol. Cells 95 (2011) 3596–3599.
[2] F. Nafezarefi, H. Schreuders, B. Dam, S. Cornelius, Photochromism of rare-earth metal-oxy-hydrides, Appl. Phys. Lett. 111 (2017), 103903.
[3] S.M. Aðalsteinsson, M.V. Moro, D. Moldarev, S. Droulias, M. Wolff, D. Primetzhofer, Correlating chemical composition and optical properties of photochromic rare-earth oxyhydrides using ion beam analysis, Nucl. Instrum. Methods Phys. Res. B 485 (2020) 36–40.
[4] C.C. You, D. Moldarev, T. Mongstad, D. Primetzhofer, M. Wolff, E.S. Marsteina, S. Zh. Karazhanova, Enhanced photochromic response in oxygen-containing yttrium hydride thin films transformed by an oxidation process, Sol. Energy Mater. Sol. Cells 166 (2017) 185–189.
[5] T. Mongstad, C. Platzer-Björkman, S. Zh. Karazhanov, A. Holt, J.P. Maehlen, B. C. Hauback, Transparent yttrium hydride thin films prepared by reactive sputtering, J. Alloys Compd. 509S (2011) S812–S816.
[6] C.C. You, T. Mongstad, J.P. Maehlen, S. Karazhanov, Dynamic reactive sputtering of photochromic yttrium hydride thin films, Sol. Energy Mater. Sol. Cells 143 (2015) 623–626.
[7] K. Kantre, M.V. Moro, D. Moldarev, M. Wolff, D. Primetzhofer, Synthesis and in-situ characterization of photochromic yttrium oxyhydride grown by reactive e−-beam evaporation, Scr. Mater. 186 (2020) 352–356.
[8] E.M. Baba, J. Montero, E. Strugovshchikov, E.Ö. Zayim, S. Karazhanov, Light-induced breathing in photochromic yttrium oxyhydrides, Phys. Rev. Mater. 4 (2020), 025201.
[9] D. Moldarev, D. Primetzhofer, C.C. You, S. Zh. Karazhanov, J. Montero, F. Martinsen, T. Mongstad, E.S. Marstein, M. Wolff, Composition of photochromic oxygen-containing yttrium hydride films, Sol. Energy Mater. Sol. Cells 177 (2018) 66–69.
[10] D. Moldarev, M.V. Moro, C.C. You, E.M. Baba, S. Zh. Karazhanov, M. Wolff, D. Primetzhofer, Yttrium oxyhydrides for photochromic applications: correlating composition and optical response, Phys. Rev. Mater. 2 (2018), 115203.
[11] S. Cornelius, G. Colombi, F. Nafezarefi, H. Schreuders, R. Heller, F. Munnik, B. Dam, Oxyhydride nature of rare-earth-based photochromic thin films, J. Phys. Chem. Lett. 10 (2019) 1342–1348.
[12] D. Moldarev, C. Aracheloff, M.V. Moro, E. Pitthan, M. Wolff, D. Primetzhofer, Oxygen mobility in yttrium hydride films studied by isotopic labelling, in: EPJ Web of Conferences 261, 2022, p. 01001.
[13] D. Moldarev, L. Stolz, M.V. Moro, S.M. Aðalsteinsson, I. Chioar, S.Zh. Karazhanov, D. Primetzhofer, M. Wolff, Environmental dependence of the photochromic effect of oxygen-containing rare-earth metal hydrides, J. Appl. Phys. 129 (2021), 153101.
[14] K. Kantre, M. Moro, D. Moldaev, D. Johansson, D. Wessmann, M. Wolff, D. Primetzhofer, SIGMA: a set-up for in-situ growth, material modification and analysis by ion beams, Nucl. Instrum. Methods Phys. Res., Sect. B: Beam Interact. Mater. Atoms 463 (2020) 96–100.
[15] P. Ström, D. Primetzhofer, Ion beam tools for nondestructive in-situ and in-operando composition analysis and modification of materials at the Tandem Laboratory in Uppsala, J. Instrum. 17 (2022) P04011.
[16] G. Hayderer, M. Schmid, P. Varga, H.P. Winter, F. Aumayr, A highly sensitive quartz-crystal microbalance for sputtering investigations in slow ion–surface collisions, Rev. Sci. Instrum. 70 (1999) 3696–3700.
[17] G. Sauerbrey, Verwendung von Schwingquarzen zur Wägung dünner Schichten und zur Mikrowägung, Zeitschrift für Physik 155 (1959) 206–222.
[18] A. Golczewski, K. Dobes, G. Wachter, M. Schmid, F. Aumayr, A quartz-crystal-microbalance technique to investigate ion-induced erosion of fusion relevant surfaces, Nucl. Instrum. Methods Phys. Res. Sect. B 267 (2009) 695–699.
[19] R. Stadlmayr, P.S. Szabo, H. Biber, H.R. Koslowski, E. Kadletz, C. Cupak, R. A. Wilhelm, M.l Schmid, C. Linsmeier, F. Aumayr, A high temperature dual-mode quartz crystal microbalance technique for erosion and thermal desorption spectroscopy measurements, Rev. Sci. Instrum. 91 (2020), 125104.
[20] J.A. Leavitt, L.C. McIntyre Jr., M.D. Ashbaugh, J.G. Oder, Z. Lin, B. Dezfouly-Arjomandy, Cross sections for 170.5° backscattering of ^{4}He from oxygen for ^{4}He energies between 1.8 and 5.0 MeV, Nucl. Instrum. Methods Phys. Res. Sect. B 44 (1990) 260–265.
[21] M. Mayer, SIMNRA, a simulation program for the analysis of NRA, RBS and ERDA, AIP Conf. Proc. 475 (1999) 541–544.
[22] A.F. Gurbich, SigmaCalc recent development and present status of the evaluated cross-sections for IBA, Nucl. Instrum. Methods Phys. Res. B 371 (2016) 27–32.
[23] M. Janson, CONTES conversion of time-energy spectra—a program for ERDA data analysis User manual, 2004.
[24] V.K. Mehta, S.C. Vogel, A.P. Shivprasad, E.P. Luther, D.A. Andersson, D.V. Rao, D. Kotlyar, B. Clausen, M.W.D. Cooper, A density functional theory and neutron diffraction study of the ambient condition properties of sub-stoichiometric yttrium hydride, J. Nucl. Mater. 547 (2021), 152837.
[25] J.F. O'Hanlon, "Gas Properties," A User's Guide to Vacuum Technology, 2003, pp. 9–24.
[26] P.S. Szabo, Experimental and Simulated Sputtering of Gold, Iron and Wollastonite with a catcher-QCM Setup, Thesis, TU Wien, 2017.
[27] D.S. Stevens, H.F. Tiersten, An analysis of doubly rotated quartz resonators utilizing essentially thickness modes with transverse variation, J. Acoust. Soc. Am. 79 (1986) 1811.